www.nature.com/cdd

CDDpress

ARTICLE

Check for updates

Upregulation of *Wilms' Tumor 1* in epicardial cells increases cardiac fibrosis in dystrophic mice

Zhenglong Guo[1,2,6], Mengyuan Geng[1,6], Yuting Huang[3], Gang Han[1], Renwei Jing[1], Caorui Lin[1], Xiaoning Zhang[4], Miaomiao Zhang[4], Guanwei Fan[3], Feng Wang[4] and HaiFang Yin[1,5]✉

Cardiomyopathy is a primary cause of mortality in Duchenne muscular dystrophy (DMD) patients. Mechanistic understanding of cardiac fibrosis holds the key to effective DMD cardiomyopathy treatments. Here we demonstrate that upregulation of Wilms' tumor 1 (*Wt1*) gene in epicardial cells increased cardiac fibrosis and impaired cardiac function in 8-month old *mdx* mice lacking the RNA component of telomerase (*mdx/mTR*$^{-/-}$). Levels of phosphorylated IκBα and p65 significantly rose in *mdx/mTR*$^{-/-}$ dystrophic hearts and Wt1 expression declined in the epicardium of *mdx/mTR*$^{-/-}$ mice when nuclear factor κB (NF-κB) and inflammation were inhibited by metformin. This demonstrates that Wt1 expression in epicardial cells is dependent on inflammation-triggered NF-κB activation. Metformin effectively prevented cardiac fibrosis and improved cardiac function in *mdx/mTR*$^{-/-}$ mice. Our study demonstrates that upregulation of *Wt1* in epicardial cells contributes to fibrosis in dystrophic hearts and metformin-mediated inhibition of NF-κB can ameliorate the pathology, and thus showing clinical potential for dystrophic cardiomyopathy. Translational Perspective: Cardiomyopathy is a major cause of mortality in Duchenne muscular dystrophy (DMD) patients. Promising exon-skipping treatments are moving to the clinic, but getting sufficient dystrophin expression in the heart has proven challenging. The present study shows that Wilms' Tumor 1 (Wt1) upregulation in epicardial cells is primarily responsible for cardiac fibrosis and dysfunction of dystrophic mice and likely of DMD patients. Metformin effectively prevents cardiac fibrosis and improves cardiac function in dystrophic mice, thus representing a treatment option for DMD patients on top of existing therapies.

Cell Death & Differentiation (2022) 29:1928–1940; https://doi.org/10.1038/s41418-022-00979-0

INTRODUCTION

Duchenne muscular dystrophy (DMD), caused by frame-shifting or point mutations in the *DMD* gene, is a fatal systemic disease affecting body-wide muscles including the heart [1]. Due to advances in respiratory support for patient care, the primary cause for mortality of DMD patients has become cardiomyopathy, characterized by extensive epicardial and myocardial fibrosis [2, 3]. It is notable that while myocardial fibrosis can be secondary to injury, fibrosis in itself is detrimental to cardiac function and thus, an important process to target therapeutically [4]. Although numerous studies have shown that multiple drugs inhibit fibrosis in skeletal muscles of DMD patients, few report effects on cardiac fibrosis [3, 5]. A better understanding of the components and processes that lead to the development of cardiac fibrosis is important for identifying therapeutic targets and developing approaches to improve cardiac function in DMD patients.

DMD patients and carriers show epicardial fibrosis even when overt muscular disease is absent [6]. Epicardium plays an important role in the heart development and regeneration and has been shown to be the source of adult cardiac progenitor cells [7]. Adult epicardial cells are reactivated and undergo epithelial-to-mesenchymal transition (EMT) and migrate to the injured area during myocardial injury [8–10]. Epicardial cells mediate and contribute to cardiac fibrosis [11], with lineage tracing studies showing that Wilms' tumor 1 (Wt1)-positive epicardial cells differentiate into fibroblasts and contribute to fibrosis in the heart [7, 12]. Also *Wt1* is involved in direct differentiation of adult epicardial cells to a default fibroblast fate after myocardial infarction [13, 14]. However, the role of *Wt1* in cardiac fibrosis of DMD remains elusive.

To understand the interplay between *Wt1* and cardiac fibrosis manifested in DMD, we assessed the expression of Wt1 protein in the epicardium of 8-month old dystrophin-deficient *mdx* mice lacking the RNA component of telomerase (*mdx/mTR*$^{-/-}$). These mice manifest severe muscular and cardiac dysfunction and fibrosis with aging, thus closely mimicking symptoms observed in DMD patients [15]. A positive correlation was established between the severity of cardiac fibrosis and levels of Wt1 expression in

[1]The Province and Ministry Co-sponsored Collaborative Innovation Center for Medical Epigenetics & Tianjin Key Laboratory of Cellular Homeostasis and Human Diseases & School of Medical Technology & Department of Cell Biology, Tianjin Medical University, Guangdong Road, Tianjin 300203, China. [2]Medical Genetic Institute of Henan Province, Henan Provincial Key laboratory of Genetic Diseases and Functional Genomics, National Health Commission Key Laboratory of Birth Defects Prevention, Henan Provincial People's Hospital, People's Hospital of Zhengzhou University, Zhengzhou 450000, China. [3]First Teaching Hospital of Tianjin University of Traditional Chinese Medicine, Changling Road, Xiqing District, Tianjin 300193, China. [4]Department of Genetics, Tianjin Medical University, Qixiangtai Road, Heping District, Tianjin 300070, China. [5]Department of Clinical Laboratory, Tianjin Medical University General Hospital, Tianjin 300052, China. [6]These authors contributed equally: Zhenglong Guo and Mengyuan Geng. ✉email: haifangyin@tmu.edu.cn

Edited by M Piacentini

Received: 24 May 2021 Revised: 4 March 2022 Accepted: 7 March 2022
Published online: 19 March 2022

dystrophic hearts of 8-month old and Wt1 over-expressing *mdx/mTR*$^{-/-}$ mice. Furthermore, nuclear factor κB (NF-κB), a master regulator of *Wt1* [16], was significantly upregulated in dystrophic hearts of 8-month old *mdx/mTR*$^{-/-}$ mice. Inhibition of NF-κB signaling pathway with metformin significantly reduced the expression of Wt1 in dystrophic hearts and improved cardiac fibrosis and function. Our study demonstrates that upregulation of *Wt1* contributes to cardiac fibrosis in DMD and thus provides a therapeutic target for DMD cardiomyopathy. These data also suggest that metformin use in DMD patients may have benefits beyond improving glucose tolerance.

MATERIALS AND METHODS

Animals

Mice were housed under specific pathogen-free conditions in a temperature-controlled room. The animal experiments were carried out in the Animal unit, Tianjin Medical University (Tianjin, China) according to procedures conformed to the guidelines from 2010/63/EU directive of the European Parliament on the protection of animals used for scientific purposes and authorized by the institutional ethical committee (permit number: SYXK 2019-0004). To generate *mdx/mTR*$^{-/-}$ mutants, congenic *C57BL/6-mTR*$^{+/-}$ (provided by Professor Feng Wang, Tianjin Medical University) and *C57BL/10ScSn-Dmd*^{mdx} mice (purchased from the Jackson Laboratory, US) were crossed to generate double-mutant mice as illustrated in Fig. S1A. Briefly, homozygous *C57BL/10 mdx* female mice were crossed with homozygous *C57BL/6-mTR*$^{-/-}$ male mice to generate *mdx/mTR*^{Het} mice. The *mdx/ mTR*^{Het} mice were further crossed to generate first generation of double mutant *mdx/mTR*$^{-/-}$ mice (F1). The *mdx/mTR*$^{-/-}$ mice (F1) were intercrossed to generate second generation of *mdx/mTR*$^{-/-}$ mice (F2). The *mdx/mTR*$^{-/-}$ mice (F2) were intercrossed to produce third generation of *mdx/mTR*$^{-/-}$ mice (F3). Only male *mdx/mTR*$^{-/-}$ mice (F3) were used in our current study. Different ages of *mdx/mTR*$^{-/-}$ mice including 2-, 4-, 6- and 8-month old and age-, gender-matched *C57BL/6* mice were used in all experiments (the number for each group was specified in Figure legends). Mice were firstly anaesthetized with 5% isoflurane (95% oxygen mix) in an induction chamber and euthanized with cervical dislocation.

Telomere quantitative fluorescence in situ hybridization (Q-FISH)

For the measurement of telomere length, 7 μm heart cryosections were fixed with 2% paraformaldehyde (PFA), followed by dehydration with gradient alcohol and air-dried. Slides were immersed in 50 μl PNA probe hybridization solution (0.25 μg/ml Cy3-labeled Telomere PNA) and denatured at 85 °C for 5 min and then hybridized at 37 °C for 2.5 h in dark, followed by washing with the washing buffer consisting of 70% formamide (Sigma, US), 10% BSA (Invitrogen, US) and 1 M Tris-HCl for twice, then with phosphate buffered saline tween-20 (PBST) for 3 times briefly. Subsequently, slides were blocked with 10% normal goat serum (NGS, Gibco, US) for 1 h and incubated with cTNT mouse monoclonal primary antibody (1:400; Invitrogen, US) for 1 h at RT, and detected with goat-anti-mouse IgG AlexFluor 488 secondary antibody (1:500, Invitrogen, US), and counterstained with DAPI for cell nuclei (DAKO, US). Z-axis was applied to determine the DAPI signal specifically located in cTNT-positive cardiomyocytes. DAPI and Cy3 signal images were acquired at 100× with Olympus FV1000 confocal microscope. Data were analyzed using the online software "Telometer: Software for Telomere Counting" (http://demarzolab.pathology.jhmi.edu/telometer/). The relative telomere length was calculated based on the ratio of the fluorescence intensity sum of all telomere pixels for a given nucleus (proportional to telomere length) to the intensity sum of DAPI pixels for the corresponding nucleus.

Isolation of epicardial cells and in vitro studies

For the isolation of epicardial cells, the epicardium was dissected from 6-8-week old or 8-month old *C57BL/6* and *mdx/mTR*$^{-/-}$ mice and rinsed in D-hanks' buffer and digested with sterilized D-hanks' buffer supplemented with 0.08% collagenase IV (Worthington, US) and 0.05% trypsin (Gibco, US) at 37 °C for 8 min under rotation (60 rpm/min) and repeated for 8 times. Subsequently, cells were centrifuged at 1000 rpm for 5 min and seeded onto 0.1% gelatin-coated 24-well plates with culture medium containing low glucose Dulbecco's modified Eagle's medium (DMEM, Invitrogen, US) and Medium 199 (M199, Invitrogen, US) in a 1:1 ratio, supplemented with 10% heat inactivated (56 °C for 25 min) fetal bovine serum (FBS, Gibco, US) and 1% penicillin / streptomycin (PS; Invitrogen, US), and cultured for 2 days or 14 days, respectively. For immortalization, mouse epicardial cells isolated from 6-8-week old *C57BL/6* mice were transfected with human telomerase (hTERT)- expressing lentivirus [17] and cells were cultured in primary epicardial cell culture medium (ECM) supplemented with 10 μM ALK5-kinase inhibitor SB431542 (Sellecks, US) to inhibit spontaneous EMT. Immortalized mouse epicardial cells (2×10^5) were plated on 6-well plates and washed carefully with DPBS without Ca^{2+}/Mg^{2+} (Invitrogen, US) prior to metformin treatment (2 mM) before or after the induction of TNF-α (50 ng/ml; Peprotech, US).

RNA extraction and RT-qPCR analysis

Total RNA was extracted with TRIzol (Invitrogen, UK) as per the manufacturer's instructions from heart tissues of metformin-treated or control *mdx/mTR*$^{-/-}$ mice, and 400 ng of RNA template was used for 20 μl of Reverse Transcription reaction with Reverse Transcription kit (Roche, US) as per the manufacturer's instructions. Quantitative PCR was performed using an Applied Biosystems StepOnePlus qPCR System with SYBR Green dye (Roche, US). The primer sequences for TNF-α were forward: 5′-GCCTCTTCTCATTCCTGCTTGTGG-3′ and reverse: 5′-CCGTTATCTCCCCTTC ATCTTCC-3′. The primer sequences for IL-1 were forward: 5′-GCACCTTACA CCTACCAGAGT-3′ and reverse: 5′-AAACTTCTGCCTGACGAGCTT-3′. The primer sequences for 18S rRNA were forward: 5′-GTAACCCGTTGAACCCC ATT-3′ and reverse: 5′-CCATCCAATCGGTAGTAGCG-3′. The homogeneity of amplicons was verified by melt curve. $2^{-\triangle\triangle CT}$ model was used for the quantitation of mRNA and 18S rRNA was used as an internal control for normalization.

Immunocytochemistry and immunohistochemistry

For immunocytochemistry, cells were seeded onto the cover slides and fixed with 4% PFA (Sigma, US) at 37 °C for 30 min, and permeabilized with 0.5% Triton X-100 (Sigma, US) for 30 min and blocked with 5% NGS for 2 h at RT, followed by the incubation of primary antibodies including Wt1 rabbit monoclonal (1:50; Abcam, US), PECAM mouse monoclonal (1:100; Abcam, US), α-SMA mouse monoclonal (1:500; Sigma, US), vimentin mouse monoclonal (1:400; Abcam, US) and FSP-1 mouse monoclonal (1:100; ProteinTech, US) at 4 °C overnight. Monoclonal or polyclonal antibodies were detected with goat anti-mouse IgG AlexFluor 488 or donkey anti-rabbit AlexFluor 594 secondary antibodies (Invitrogen, US), respectively, at a dilution of 1:200 at RT for 1 h. The nuclei were counterstained with DAPI (DAKO, US). For immunohistochemistry, 7 μm heart cryosections were blocked with 10% NGS at RT for 2 h and detected with Wt1 rabbit monoclonal primary antibody (1:50; Abcam, US), PECAM mouse monoclonal primary antibody (1:100; Abcam, US), α-SMA mouse monoclonal primary antibody (1:500; sigma, US), vimentin mouse monoclonal primary antibody (1:400; Abcam, US) and cTNT mouse monoclonal primary antibody (1:400; Invitrogen, US), then were detected with goat anti-mouse IgG AlexFluor 488 or donkey anti-rabbit AlexFluor 594 secondary antibodies (Invitrogen, US), respectively, at a dilution of 1:200 at RT for 1 h. Staining of dystrophin and CD68-positive macrophage was the same as described previously [18]. Briefly, dystrophin was probed with a rabbit polyclonal primary antibody (1:3000; Abcam, US) and CD68-positive macrophages were stained with rabbit polyclonal antibody (1:500; Abcam, US) and then detected by goat anti-rabbit IgG AlexaFluor 594 secondary antibody (Invitrogen, US).

Protein extraction and western blot

For protein extraction, the collected tissue sections or mouse epicardial cells were placed in a 1.5 ml polypropylene eppendorf tube (Anachem, UK) on dry ice and lysed with 150 μl protein extraction buffer containing 125 mmol/l Tris–HCl (pH = 6.8), 10% sodium dodecyl sulphate (SDS), 2 mol/l urea, 20% glycerol and 5% 2-mercaptoethanol. Subsequently, the mixture was boiled for 5 min and centrifuged, and then the supernatant was collected and the protein concentration was quantified by Bradford assay (Sigma, US). Various amounts of protein from *C57BL/6* and *mdx/mTR*$^{-/-}$ mice and mouse epicardial cell lysates were loaded onto SDS polyacrylamide gel electrophoresis gels (4% stacking, 10% resolving). Samples were electrophoresed for 2.5 h at 80 V and transferred to nitrocellulose for 2 h at 250 mA at 4 °C. The membrane was then washed and blocked with 5% skimmed milk and probed overnight with rabbit monoclonal primary antibodies including Wt1 (1:1000; Abcam, US), PECAM (1:000; Abcam, US), α-SMA (1:1000; Abcam, US), p-AMPK (1:1000; Abcam, US), AMPK (1:1000; Abcam, US), E-cadherin (1:1000;

Proteintech, US), vimentin mouse monoclonal primary antibody (1:1000; Abcam, US), flag rabbit polyclonal primary antibody (1:5000; Sigma, US), CTGF rabbit polyclonal primary antibody (1:1000; Abcam, US) and collagen rabbit polyclonal primary antibody (1:1000; Proteintech, US) for the detection of Wt1, PECAM, α-SMA, AMPK, p-AMPK, E-cadherin, vimentin, flag, CTGF and type III collagen protein. p65 and IκBα were detected by primary antibodies including: p-p65 rabbit polyclonal antibody (1:1000; Abcam, US), p65 mouse monoclonal antibody (1:1000; Ruiying Biological, China), p-IκBα rabbit monoclonal antibody (1:1000; Abcam, US), IκBα rabbit monoclonal antibody (1:1000; Abcam, US). GAPDH (mouse monoclonal antibody, 1:3000, Proteintech, US), β-actin (rabbit polyclonal antibody, 1:3000, Proteintech, US) or α-actinin (mouse monoclonal antibody, 1:3000, Sigma, US) was used as a loading control. The bound primary antibody was detected by horseradish peroxidase conjugated goat anti-mouse IgGs or goat anti-rabbit IgGs (1:5000; MULTI-SCIENCES, China) and developed by the ECL Western Blotting Analysis system (Amersham Pharmacia Biosciences, UK). The intensity of the bands obtained from heart tissues was measured by Image J software; the quantification is based on band intensity and area, and is compared with that from wild-type controls after normalization. All of the original western blots were included in the "original data file".

Histology and Masson's trichrome staining

Routine Hematoxylin & Eosin staining was performed. Masson's trichrome staining kit (Solarbio, China) was applied for the collagen staining as per the manufacturer's instructions. Briefly, series of 8 μm sections were fixed overnight in Bouin's solution, followed by staining with the kit as per the manufacturer's instructions. The images were captured with Pannoramic DESK digital slide-scanner (3D HISTECH, Hungary). The collagen-positive area was measured by Image J software and 3 sections per mouse and 3-6 mice per group were measured. For each section, the ratio between the collagen-positive area and total area of sections was calculated.

Cardiac function measurements

Cardiac structure and function were assessed by echocardiography. Briefly, mice were anaesthetized with 5% isoflurane (95% oxygen mix) in an induction chamber. And echocardiography was performed on different ages of *C57BL/6* and *mdx/mTR*$^{-/-}$ mice in mono-dimensional mode (M-Mode) with a high-resolution transducer at a frequency of 30 MHz (VisualSonics Vevo770, Canada). Mice were held in the supine position and anesthetized by isoflurane with the anterior chest wall shaved. Warm ultrasound gel was applied to the shaved chest and the transducer probe was placed over left hemithorax. Parasternal and short-axis two dimensional images of left ventricle were acquired to determine the correct M-Mode cursor positioning. Multiple short axis M-Mode images were acquired and analyzed for left ventricle function. The heart rate was determined from at least three consecutive RR intervals. The left ventricle M-Mode trace was used to measure ejection fraction (EF) and shortening fraction (FS). LV diastolic function including the isovolumic relaxation time (IVRT), mitral inflow E and A wave ratio (E/A) was evaluated using Pulse Wave Doppler by imaging Transmitral inflow.

Serum enzyme measurements

Mouse blood was taken immediately after cervical dislocation and centrifuged at 1500 rpm for 30 min. Serum was separated and stored at −80 °C. Analysis of levels of serum creatine kinase (CK), aspartate aminotransferase (AST) and alanine transaminase (ALT) and CK-MB was performed in the clinical laboratory (Tianjin Metabolic Disease Hospital, Tianjin Medical University).

Grip strength test

Treated and control mice were tested using a commercial grip strength monitor (Chatillon). Briefly, each mouse was held 2 cm from the base of the tail, allowed to grip a protruding metal triangle bar attached to the apparatus with their forepaws, and pulled gently until they released their grip. The force exerted was recorded, and five sequential tests were carried out for each mouse, averaged at 30 s apart. Subsequently, the readings for force recovery were normalized by the bodyweight.

AAV generation

Murine *Wt1* gene (Genebank no. NM_144783.2) was cloned into recombinant adeno-associated virus (serotype 9) vectors with 3×flag tagged ZsGreen fluorescent protein (ZsGreen) (AAV9-CMV-Wt1-3×flag-ZsGreen) as illustrated in Figure S4A and the virus was purchased from Hanbio Inc (Shanghai, China). AAV9-CMV-ZsGreen was used as a negative control. AAV9-CMV-Wt1-3 × flag-ZsGreen or AAV9-CMV- ZsGreen (1.5×10^{11} vector genomes (vg) per mouse) was injected into 4 month old *mdx/mTR*$^{-/-}$ mice intravenously for once. Tissues were harvested 2 months after injection.

Metformin treatment

Metformin hydrochloride (1-dimethylbiguanide hydrochloride, Meilunbio, China) was formulated in filtered tap water and administered into 6-month old *mdx/mTR*$^{-/-}$ mice orally via gavage at a dose of 500 mg/kg/day for 2 months, a protocol adopted from previous studies [19]. Mice were monitored during the experimental period and tissues were harvested 2 months later.

Statistical analysis

All data are reported as mean values ± s.e.m. Statistical differences between different treatment groups were evaluated by Sigma Stat (Systat Software Inc., Chicago, IL, US). Both parametric and non-parametric analyses were applied as specified in figure legends. Significance was determined based in $p < 0.05$.

RESULTS

Upregulation of *Wt1* in epicardial cells increases fibrosis in dystrophic hearts

To better model cardiac fibrosis manifested in DMD patients, we generated double mutant dystrophic *mdx* mice lacking telomerase activity by crossing *mdx* female mice homozygous for the *dmd* mutation [20] with *C57BL/6* mice homozygous for the telomerase RNA component Terc (*mTR*$^{-/-}$) [15] (Fig. S1A). Consistent with previous observations [15], the resulting *mdx/mTR*$^{-/-}$ mice showed significantly shortened telomeres (Fig. S1B, S1C) compared to wild-type and *mdx* mice and the absence of dystrophin expression (Fig. S1D). In particular, the third generation (F3) manifested the most pronounced phenotypes demonstrated by increased muscle degeneration (Fig. S1E), and significantly increased levels of creatine kinase (CK), aspartate aminotransferase (AST) and alanine transaminase (ALT) (Fig. S1F). Examination of the pathological progression of *mdx/mTR*$^{-/-}$ mice (F3) revealed marked cardiac functional impairments and fibrosis at 8 months reflected by significantly reduced ejection fraction (EF) and fractional shortening (FS) (Fig. S2A), and substantial collagen deposition (Fig. S2B), therefore 8-month old *mdx/mTR*$^{-/-}$ mice were used for subsequent studies.

In infarcted hearts, *Wt1* was shown to be upregulated in the epicardium and Wt1-positive epicardial cells appeared to differentiate into fibroblasts and contributed to fibrosis [11, 12]. Thus we hypothesized that *Wt1* may play a role in cardiac fibrosis of DMD and examined Wt1 expression in 8 month old *mdx/mTR*$^{-/-}$ mouse hearts. Levels of Wt1 protein (Fig. 1A, B) and numbers of Wt1-positive epicardial cells (Fig. 1C, D) were significantly elevated compared to age-matched wild-type mice. Consistent with previous observations [11], a substantial number of vimentin-positive fibroblasts [21] was detected in the epicardium (Fig. 1E) and myocardium (Fig. S3A) of dystrophic hearts in close proximity of Wt1-positive cells, whereas there was no evident difference in platelet endothelial cell adhesion molecule (PECAM-1)-positive endothelial cells [22] and α-smooth muscle actin (α-SMA)-positive smooth muscle cells [23] in the hearts from 8-month old *mdx/mTR*$^{-/-}$ and age-matched wild-type controls (Figs. 1E and S3A). Concordantly, the expression of vimentin significantly rose in dystrophic hearts compared to age-matched wild-type controls (Fig. 1F). Staining of epicardial cells isolated from the hearts of 8 month old *mdx/mTR*$^{-/-}$ and age-matched wild-type mice revealed comparable numbers of Wt1-positive epicardial cells in *mdx/mTR*$^{-/-}$ mice (53.3 ± 2.9%) and wild-type controls (47.5 ± 4.1%), with the appearance of epithelium-like morphologies on day 2, whereas a large proportion of epicardial cells from *mdx/*

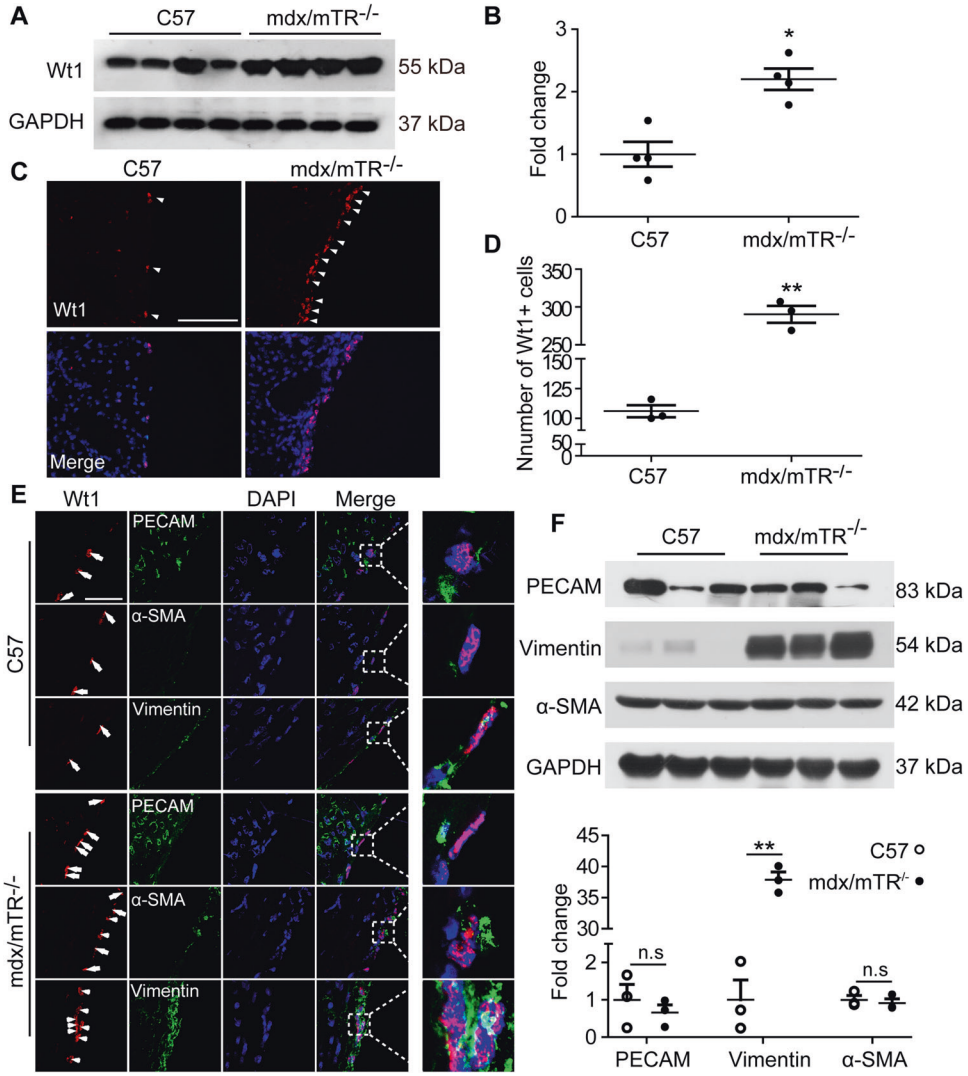

Fig. 1 Evaluation of Wt1 expression in the hearts of 8-month old *mdx/mTR*$^{-/-}$ mice. A Western blots to show the expression of Wt1 protein in dystrophic hearts of 8-month old *mdx/mTR*$^{-/-}$ mice. Total protein (50 μg) was loaded and GAPDH was used as a loading control. **B** Quantitative analysis of Wt1 expression in dystrophic hearts. Fold change refers to the Wt1 expression in 8-month old *mdx/mTR*$^{-/-}$ mice relative to age-matched *C57BL/6* mice ($n = 4$, $^{*}p < 0.05$; two-tailed t test). **C** Immunostaining of Wt1 in the epicardium of 8-month-old *mdx/mTR*$^{-/-}$ mice (scale bar = 100 μm). Arrowheads point to Wt1-positive epicardial cells. Nuclei were counterstained with DAPI (blue). **D** Quantitative analysis of Wt1-positive epicardial cells in dystrophic hearts ($n = 3$, $^{**}p < 0.001$; two-tailed t-test). Whole ventricular epicardium areas of each section were counted for each mouse and 3 mice for each group were examined. **E** Immunostaining of different marker proteins in the epicardium of 8-month old *mdx/mTR*$^{-/-}$ mice (scale bar = 10 μm). Boxed areas were magnified. **F** Western blots to examine the expression of different proteins in dystrophic hearts and quantitative analysis of different protein expression. Total protein (50 μg) was loaded and GAPDH was used as a loading control. Fold change refers to different protein expression in 8-month old *mdx/mTR*$^{-/-}$ mice relative to age-matched *C57BL/6* mice ($n = 3$, $^{**}p < 0.001$; two-tailed t-test). N.s means not significant. Data are presented as mean ± s.e.m in (**B**), (**D**) and (**F**).

mTR$^{-/-}$ mice showed spindle-like shape (Fig. 2A and B), suggesting that epicardial cells are activated and undergo EMT transformation, a feature unique to activated Wt1-positive epicardial cells [24, 25]. Consistently, Wt1-positive epicardial cells derived from dystrophic epicardium dramatically dropped to approximately 14% of total cells on day 14, with the majority of cells manifesting spindle-shaped morphologies (Fig. 2A). Corroborating with morphological changes, staining of spindle-shaped cells from dystrophic epicardium confirmed the presence of fibroblast-specific protein (FSP1) [26] -positive fibroblasts on day 14 (Fig. 2C), indicating that Wt1-positive epicardial cells differentiated into fibroblasts. In contrast, Wt1-positive epicardial cells from wild-type mice retained epithelial morphology without obvious fibroblast differentiation (Figs. 2A and S3B), implying that Wt1-positive epicardial cells from wild-type mice remain quiescent [24]. Correspondingly, focal areas of fibrosis were present in the epicardium and myocardium of 8-month old *mdx/mTR*$^{-/-}$ mice revealed by Masson's trichrome staining (Fig. 2D), covering approximately 30% of total stained area, whereas a negligible level of fibrosis was detected in the hearts of age-matched wild-type mice (Fig. 2E). These data demonstrated that *Wt1* is upregulated in the epicardium and Wt1-positive epicardial cells differentiate into fibroblasts, resulting in cardiac fibrosis in dystrophic mice.

Over-expression of Wt1 exacerbates cardiac fibrosis in dystrophic mice

To confirm the critical role of *Wt1* in cardiac fibrosis of DMD, we hypothesized that the introduction of Wt1 prior to the onset of cardiac fibrosis would increase fibrosis. Therefore we transduced 4-month old *mdx/mTR*$^{-/-}$ mice, an age showing negligible level of cardiac fibrosis (Fig. S2B), with *Wt1*-expressing adeno-associated

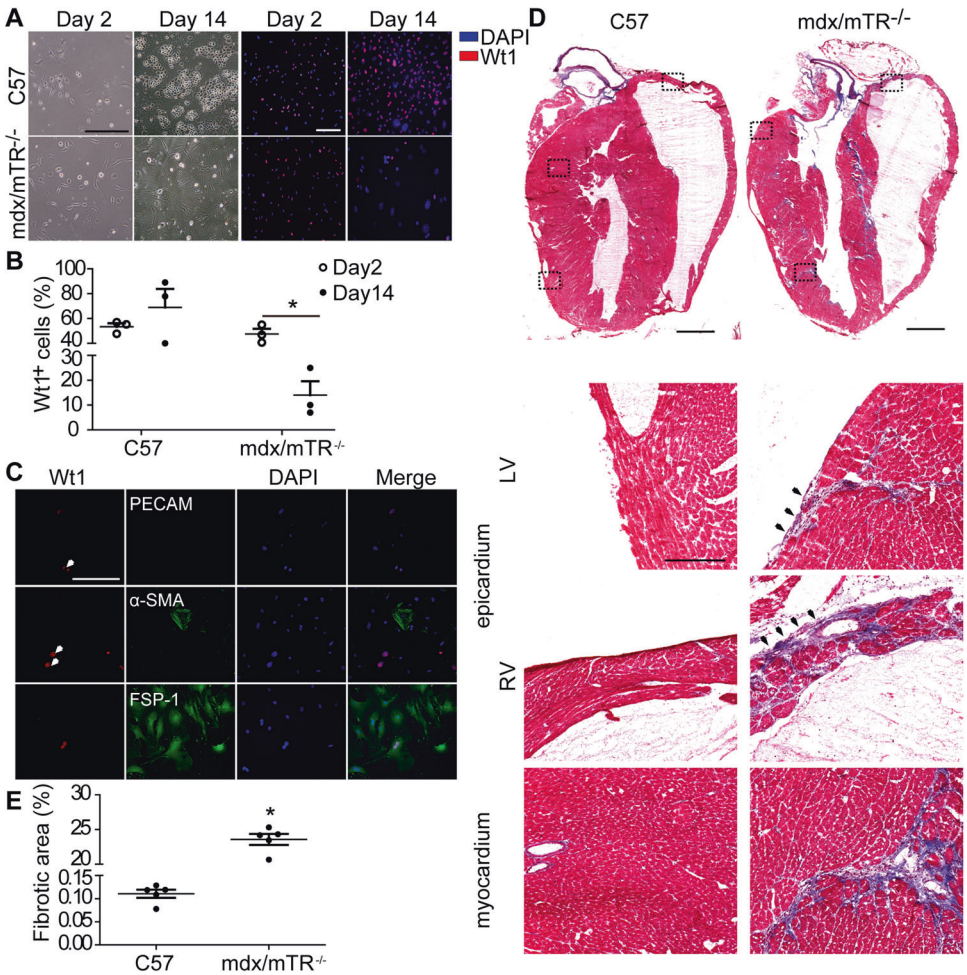

Fig. 2 In vitro characterization of epicardial cells and examination of cardiac fibrosis in 8-month old *mdx/mTR*$^{-/-}$ mice. A Immunocytochemistry of Wt1 protein in isolated epicardial cells from 8-month old *mdx/mTR*$^{-/-}$ mice at different time-points (scale bar = 100 μm). **B** Quantitative analysis of Wt1-positive epicardial cells at day 2 and day 14 ($n = 3$, $^*p < 0.05$; two-tailed t-test). **C** Immunocytochemistry of different marker proteins in isolated epicardial cells from 8-month old *mdx/mTR*$^{-/-}$ mice at day 14 (scale bar = 100 μm). Arrowheads point to Wt1-positive epicardial cells. **D** Representative images for collagen deposition in the whole heart (scale bar = 500 μm) and magnified areas for the epicardium and myocardium from 8-month old *mdx/mTR*$^{-/-}$ mice (scale bar = 100 μm). The boxed areas were magnified and arrowheads point to collagen-positive areas. **E** Quantitative analysis of fibrotic (collagen-positive) areas in dystrophic hearts from 8-month old *mdx/mTR*$^{-/-}$ mice ($n = 5$, $^*p < 0.05$; Mann-Whitney U test). Data are presented as mean ± s.e.m in (**B**) and (**E**).

virus 9 (AAV9) (Fig. S4A), a serotype is known to infect the heart effectively [27], and harvested tissues 2 months later. As expected, levels of total Wt1 protein were significantly increased in the hearts from *mdx/mTR*$^{-/-}$ mice transduced with *Wt1*-expressing AAVs compared to control mice transduced with empty vectors (Fig. 3A). Notably, there was no difference in the level of endogenous Wt1 expression between empty vector transduced and 6-month old *mdx/mTR*$^{-/-}$ mice (Fig. S4B), suggesting that AAV does not have any impact on the endogenous Wt1 expression nor cause inflammation sufficient to trigger fibrosis. Correspondingly, Wt1-positive cells significantly rose in the epicardium of *mdx/mTR*$^{-/-}$ mice transduced with *Wt1*-expressing AAVs compared to controls (Fig. 3B). Unsurprisingly, Wt1 expression was also visible in the myocardium of *mdx/mTR*$^{-/-}$ mice transduced with *Wt1*-expressing AAVs (Fig. S4C). Importantly, over-expression of Wt1 exacerbated cardiac fibrosis of *mdx/mTR*$^{-/-}$ mice as shown by pronounced collagen staining (Fig. 3C, D) and resulted in deteriorated cardiac function reflected by significantly decreased EF and FS rates, and increased left ventricular internal diameter at end-diastole (LVIDD) in the hearts of *Wt1*-transduced *mdx/mTR*$^{-/-}$ mice compared to blank AAV9 controls, whereas there was no difference between blank AAV9-transduced and age-matched untreated *mdx/mTR*$^{-/-}$ controls (Fig. 3E, F). These results strengthened the conclusion that upregulation of *Wt1* increases cardiac fibrosis in dystrophic mice.

Inflammation-induced NF-κB activation positively correlates to Wt1 expression in dystrophic epicardium

It was reported that *Wt1* is one of the target genes modulated by nuclear factor-kappa B (NF-κB) [16] and NF-κB signaling factor is a master regulator of inflammatory responses in DMD skeletal muscles [28]. To investigate whether NF-κB is involved in *Wt1* activation in dystrophic hearts, we examined phosphorylated IκBα and p65, two key indicators for activation of NF-κB signaling pathway [29], in 8-month old *mdx/mTR*$^{-/-}$ mouse hearts. The results showed significantly higher ratios of phosphorylated IκBα and p65 relative to total protein in dystrophic hearts compared to age-matched wild-type controls (Fig. 4A, B), indicating NF-κB activation in dystrophic hearts. Since cardiac fibrosis increased with age in *mdx/mTR*$^{-/-}$ mice (Fig. S2B), we next examined whether there is any correlation between Wt1-positive epicardial cell counts and levels of NF-κB activation in the hearts from different ages of *mdx/mTR*$^{-/-}$ mice. Unsurprisingly, the abundance of Wt1-positive epicardial cells (Fig. 4C, D) positively correlated to NF-κB activation

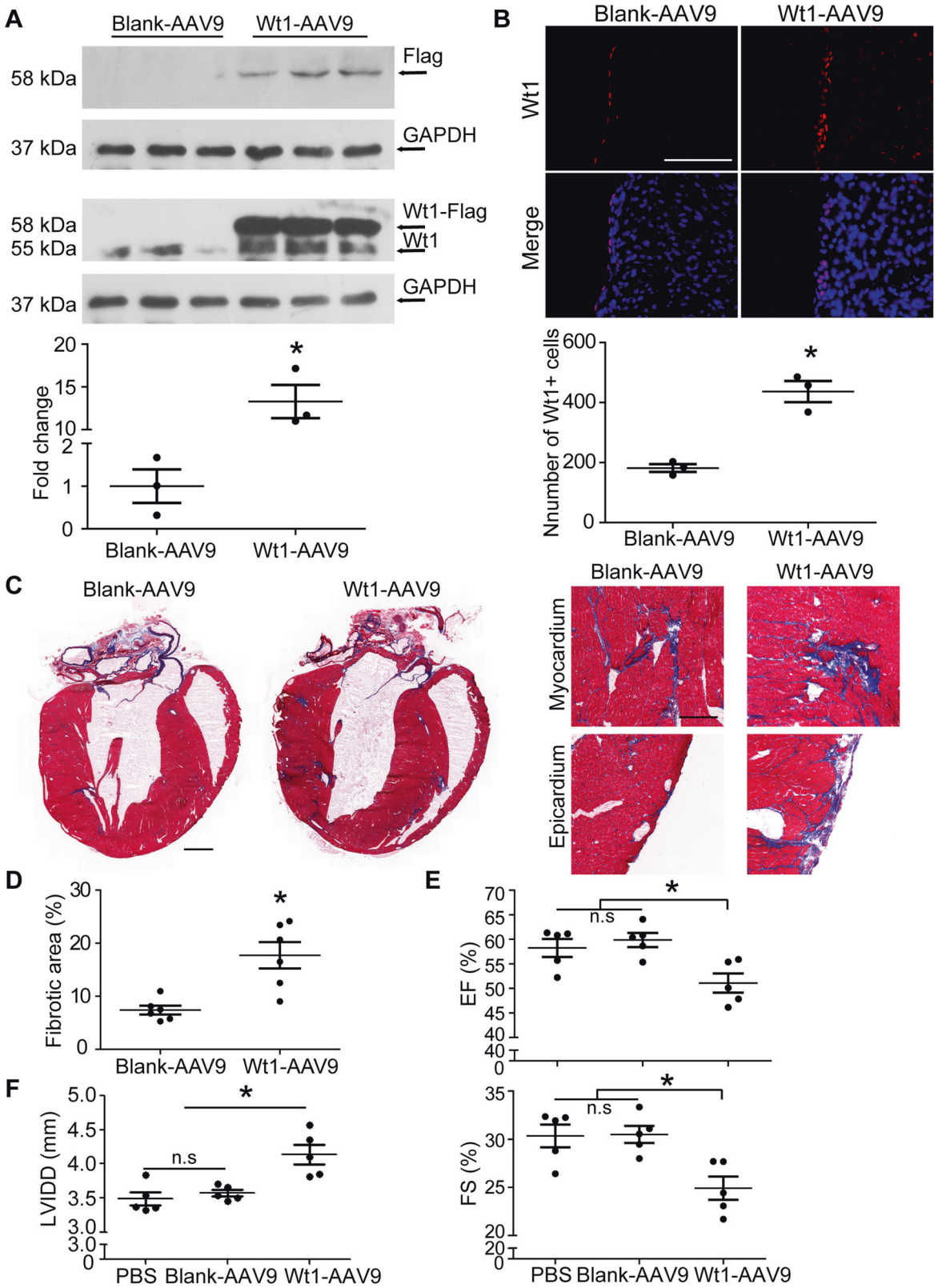

in dystrophic hearts reflected by significantly increased ratios of phosphorylated IκBα and p65 relative to total protein in 8-month old compared to 6-, 4- and 2-month old *mdx/mTR*$^{-/-}$ mice (Fig. 4E, F), further confirming the involvement of NF-κB activation in *Wt1* upregulation. Since pro-inflammatory cytokines such as tumor necrosis factor α (TNF-α) and interleukin 1 (IL-1), predominantly elevated in DMD patients [30], were known to trigger NF-κB activation [31], we measured levels of TNF-α and IL-1 expression in dystrophic hearts from *mdx/mTR*$^{-/-}$ mice of different ages. Notably, levels of TNF-α and IL-1 expression significantly rose with age in *mdx/mTR* $^{-/-}$

Fig. 3 Systemic investigation of the effect of Wt1 over-expression on cardiac fibrosis and function in *mdx/mTR*$^{-/-}$ mice. *Wt1*-expressing AAV9 was administered into 4-month old *mdx/mTR*$^{-/-}$ mice intravenously and tissues were harvested 2 months later. **A** Western blots to examine the expression of and quantitative analysis of Wt1 protein in dystrophic hearts of *Wt1*-expressing AAV9-transduced *mdx/mTR*$^{-/-}$ mice. Total protein (50 μg) was loaded and GAPDH was used as a loading control. Wt1-Flag refers the exogenous Wt1. Fold change refers to the total Wt1 (exogenous and endogenous) expression in the hearts of *Wt1*-expressing AAV9-transduced *mdx/mTR*$^{-/-}$ mice relative to age-matched blank AAV controls ($n = 3$, $^*p < 0.05$; two-tailed t test). **B** Immunostaining of Wt1 in the epicardium and quantitative analysis of Wt1-positive epicardial cells in *Wt1*-expressing AAV9-transduced *mdx/mTR*$^{-/-}$ mice (scale bar = 100 μm) ($n = 3$, $^*p < 0.05$; two-tailed t test). **C** Representative images for collagen deposition in the whole heart (scale bar = 500 μm) and magnified areas for the epicardium and myocardium from Wt1 over-expressing *mdx/mTR*$^{-/-}$ mice (scale bar = 100 μm). The boxed areas were magnified. **D** Quantitative analysis of fibrotic (collagen-positive) areas in dystrophic hearts from Wt1 over-expressing *mdx/mTR*$^{-/-}$ mice ($n = 6$, $^*p < 0.05$; Mann-Whitney U test). Measurement of Ejection Fraction (EF, $F = 7.067$, $P = 0.009$) and Fractional Shortening (FS, $F = 8.289$, $P = 0.005$) (**E**) and left ventricular internal diameter at end-diastole (LVIDD, $F = 11.752$, $P = 0.001$) (**F**) in 6-month old *Wt1*-expressing AAV9-transduced *mdx/mTR*$^{-/-}$ mouse hearts with echocardiography ($n = 5$, $^*p < 0.05$, $^{**}p < 0.001$; one-way ANOVA post hoc Student-Newman-Keuls test). EF and FS refer to ejection fraction and fractional shortening, respectively. N.s means not significant. Data are presented as mean± s.e.m in (**A**), (**B**), (**D**), (**E**) and (**F**).

mice (Fig. 4G), suggesting that inflammation-triggered NF-κB activation contributes to *Wt1* upregulation in epicardial cells of dystrophic hearts.

Metformin inhibits NF-κB and prevents *Wt1* upregulation in dystrophic hearts

Metformin was known to be a potent inhibitor for pro-inflammatory cytokine-induced NF-κB activation [32]. To determine if blockade of NF-κB signaling pathway with metformin can prevent *Wt1* upregulation, we orally administered metformin at the dose of 500 mg/kg/day for 2 months in 6-month old *mdx/mTR*$^{-/-}$ mice, a dosing regimen adopted from the previous study [19]. Activation of NF-κB was effectively inhibited as demonstrated by significantly decreased ratios of phosphorylated IκBα and p65 relative to total protein in metformin-treated dystrophic hearts compared to age-matched untreated controls (Fig. 5A, B), to a level comparable to pretreated mice, indicating that metformin effectively inhibits NF-κB activation. Unsurprisingly, levels of TNF-α and IL-1 expression significantly declined in dystrophic hearts from metformin-treated mice compared to untreated age-matched controls (Fig. S5A), suggesting that metformin improves inflammatory conditions. The level of Wt1 expression also significantly declined (Fig. 5C) and the number of Wt1-positive epicardial cells (Fig. 5D and E) dramatically decreased in metformin-treated *mdx/mTR*$^{-/-}$ mouse hearts compared to untreated age-matched controls. Importantly, there was no difference in Wt1 expression between pretreated 6-month old and metformin-treated 8-month old *mdx/mTR*$^{-/-}$ mice (Fig. 5C–E), indicating that blockade of NF-κB activation effectively prevents *Wt1* upregulation. Notably, blockade of inflammatory cytokine-induced NF-κB activation was accompanied by Wt1 downregulation and AMPK activation (Fig. S5B, S5C), which is upstream of NF-κB inhibition [33, 34], in mouse epicardial cells in vitro. This suggests that metformin inhibited inflammation-triggered NF-κB activation via activating AMPK pathway. Concordantly, EMT transformation was dramatically inhibited, reflected by significantly increased α-SMA and decreased E-cadherin (E-cad) (Fig. S5D), an epithelial marker [35] in metformin-treated mouse epicardial cells in vitro. These findings strengthen the conclusion that inflammation triggers NF-κB activation and leads to *Wt1* upregulation in dystrophic hearts.

Metformin improves cardiac fibrosis and function in dystrophic mice

Since metformin effectively prevented the activation of *Wt1*, we next examined whether metformin has any impact on cardiac fibrosis. Strikingly, cardiac fibrosis was significantly alleviated with metformin treatment compared to age-matched untreated controls reflected by Masson's trichrome staining (Fig. 6A, B) and reduced collagen expression (Fig. 6C, D), to an extent similar to pretreated conditions (Fig. 6A–D). Consequently, cardiac function was significantly improved as demonstrated by significantly elevated EF and FS rates and reduced LVIDD (Fig. 6E, F), and significantly increased ratio of peak early (E) and peak atrial filling velocity (A) (E/A) and decreased isovolumetric relaxation time (IVRT) (Fig. 6G), two widely used indices of assessing diastolic function in DMD [36–38], and decreased levels of serum creatine kinase-MB (CK-MB) (Fig. 6H), an enzyme primarily found in the heart and is released during cardiac damage [39], in metformin-treated *mdx/mTR*$^{-/-}$ mice compared to age-matched untreated controls. Importantly, metformin effectively prevented cardiac functional deterioration with age as there was no difference observed in EF and FS rates, LVIDD, E/A ratio and IVRT between metformin-treated 8-month old and pretreated 6-month old *mdx/mTR*$^{-/-}$ mice (Fig. 6E–G), indicating the potency of metformin in preventing the pathological progression of dystrophic hearts.

Unsurprisingly, metformin treatment elicited phenotypic rescue in skeletal muscles evidenced by significantly increased grip strength compared to age-matched untreated controls (Fig. S6A). Also metformin dramatically reduced levels of serum CK, ASL and ALT compared to pretreated and age-matched untreated controls (Fig. S6B, S6C). Consistent with previous reports [40], muscle pathologies were improved as evidenced by decreased fibrosis and infiltration of macrophages, immune cells predominantly elevated in dystrophic muscles [41], in diaphragms of metformin-treated *mdx/mTR*$^{-/-}$ mice compared to pretreated and age-matched untreated controls (Fig. S6D), indicating that metformin has a profound effect on skeletal muscles. Altogether, these data demonstrate that metformin can effectively prevent disease progression in body-wide muscles including the hearts of *mdx/mTR*$^{-/-}$ mice.

DISCUSSION

Cardiomyopathy, primarily presented as cardiac fibrosis, represents a daunting task for the treatment of DMD [2]. Therefore, elucidating the mechanism underpinning cardiac fibrosis is critical for developing more effective treatments for DMD. Here, we uncovered the role of *Wt1* in cardiac fibrosis of DMD and demonstrated that upregulation of *Wt1* in the epicardium contributes to cardiac fibrosis in dystrophic mice. This notion was further strengthened by Wt1 over-expression, which worsened cardiac fibrosis and function in *mdx/mTR*$^{-/-}$ mice, suggesting that *Wt1* might be a potential therapeutic target for DMD cardiomyopathy. Elucidation of the molecular mechanism underpinning *Wt1* upregulation unveiled that inflammation-induced NF-κB activation is largely responsible for the upregulation of *Wt1* as demonstrated by age-related increase in the expression of Wt1 and activation of NF-κB in *mdx/mTR*$^{-/-}$ mice. The reduction of inflammation and subsequent blockade of NF-κB with metformin completely abrogated the expression of Wt1 in *mdx/mTR*$^{-/-}$ mice (Fig. 7). Importantly, metformin treatment significantly improved cardiac and muscular function in *mdx/mTR*$^{-/-}$ mice and thus opens up a new therapeutic avenue for DMD patients.

Wt1 is an important transcription factor for the development of kidney, genitourinary system, mesothelium and heart [42]. Recently, Wt1 has also been shown to be upregulated in pleural

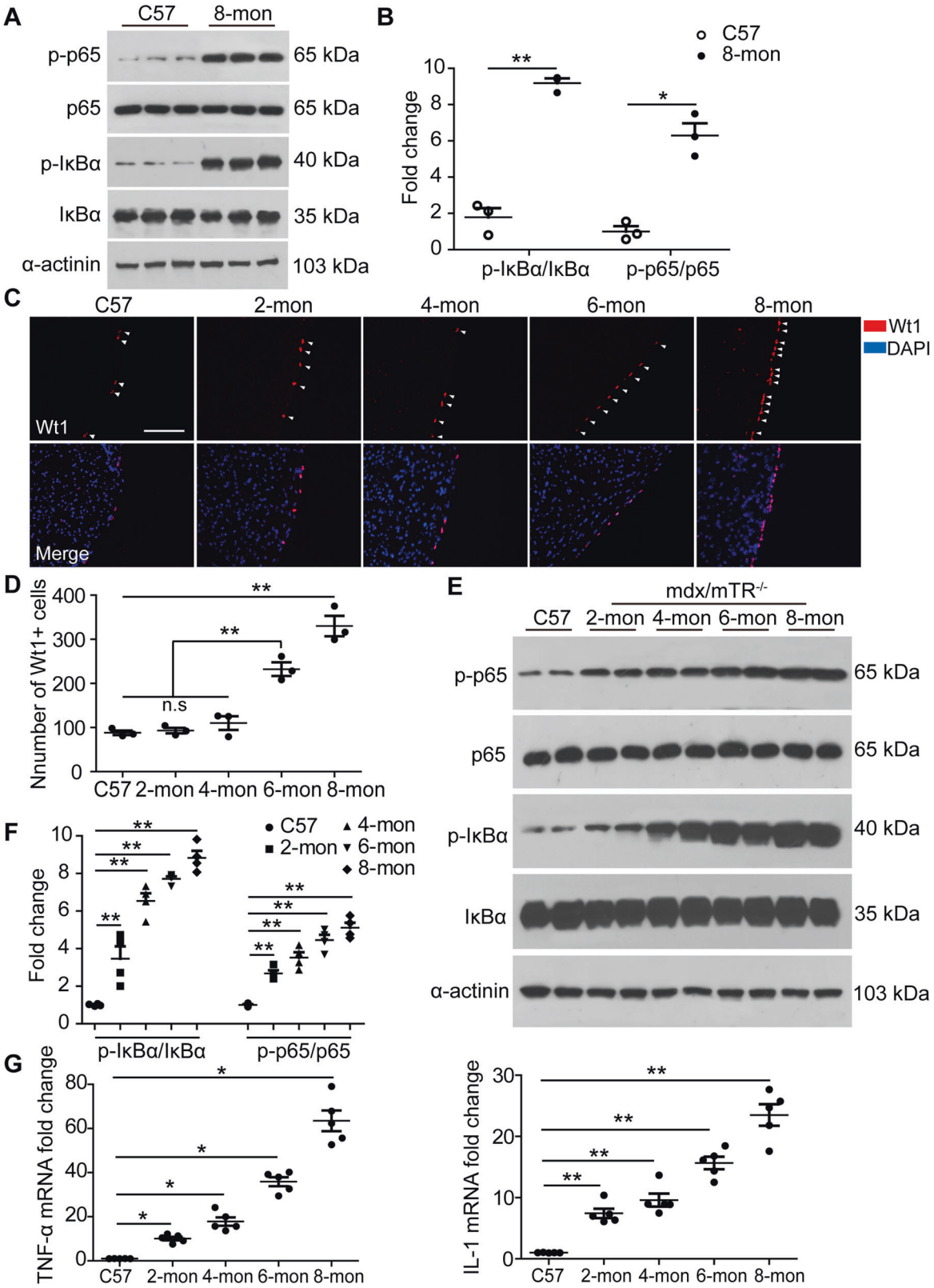

mesothelial cells and promote mesothelial-to-myofibroblast transformation (MMT), and thus contribute to the pathogenesis of lung fibrosis of idiopathic pulmonary fibrosis (IPF) [43–45], which further supports our conclusion that Wt1 upregulation and activation is primarily responsible for cardiac fibrosis of DMD. In addition, Wt1 expression was shown to be restricted to the epicardium and declined with the developmental stages of the heart [46]. It is notable that Wt1-positive epicardial cells appear to be a major contributor to cardiac fibrosis not only in DMD but also in cardiac infarction using wild-type models [11, 14, 24],

Fig. 4 Examination on NF-κB activation and Wt1 expression in different ages of *mdx/mTR*$^{-/-}$ mice. A Western blots to examine the expression of phosphorylated and total protein expression of p65 and IκBα in dystrophic hearts of 8-month old *mdx/mTR*$^{-/-}$ mice. Total protein (100 μg) was loaded and α-actinin was used as a loading control. **B** Quantitative analysis of phosphorylated p65 and IκBα in dystrophic hearts ($n = 3$, $^{*}p < 0.05$, $^{**}p < 0.001$; two-tailed t test). Fold change refers to phosphorylated p65 and IκBα relative to total protein expression in 8-month old *mdx/mTR*$^{-/-}$ mice compared to *C57BL/6* controls. **C** Immunostaining of Wt1 in the epicardium from different ages of *mdx/mTR*$^{-/-}$ mice (scale bar = 100 μm). Arrowheads point to Wt1-positive epicardial cells. **D** Quantitative analysis of Wt1-positive epicardial cells in different ages of *mdx/mTR*$^{-/-}$ mice ($n = 3$, $^{**}p < 0.001$; one-way ANOVA post hoc Student-Newman-Keuls test, $F = 53.292$, $P < 0.001$). N.s means not significant. **E** Representative western blots to examine the expression of phosphorylated and total protein expression of p65 and IκBα in dystrophic hearts from different ages of *mdx/mTR*$^{-/-}$ mice. Total protein (100 μg) was loaded and α-actinin was used as a loading control. **F** Quantitative analysis of phosphorylated p65 ($F = 48.017$, $P < 0.001$) and IκBα ($F = 69.076$, $P < 0.001$) in dystrophic hearts from different ages of *mdx/mTR*$^{-/-}$ mice ($n = 4$, $^{**}p < 0.001$; one-way ANOVA post hoc Student-Newman-Keuls test). Fold change refers to phosphorylated p65 and IκBα relative to total protein expression in 8-month old *mdx/mTR*$^{-/-}$ mice compared to *C57BL/6* controls. **G** Measurements of expression levels of inflammatory cytokines including TNF-α ($F = 99.957$, $P < 0.001$) and IL-1 ($F = 62.433$, $P < 0.001$) in dystrophic hearts from different ages of *mdx/mTR*$^{-/-}$ mice ($n = 5$, $^{*}p < 0.05$, $^{**}p < 0.001$; one-way ANOVA post hoc Student-Newman-Keuls test). The expression level of TNF-α or IL-1 in *C57BL/6* mice was set as 1. Data are presented as mean ± s.e.m in (**A**), (**B**), (**D**), (**F**), and (**G**).

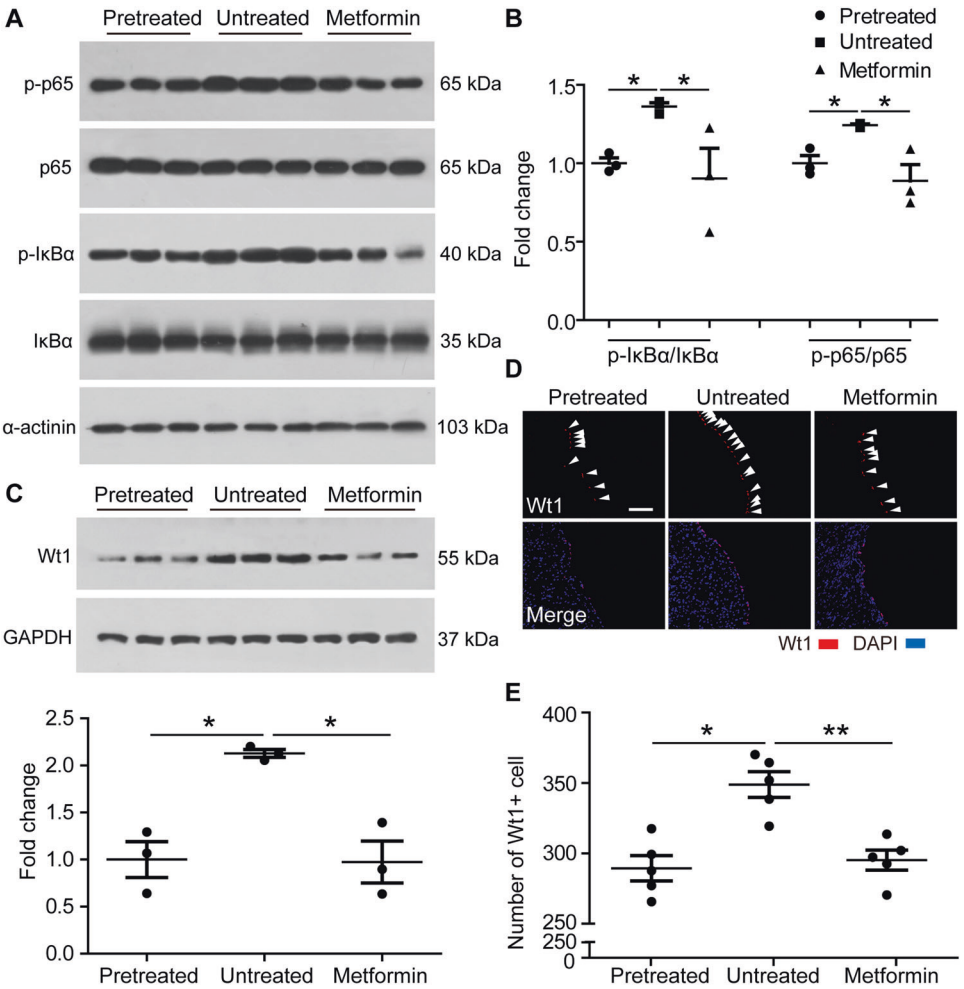

Fig. 5 Investigation of NF-κB activation and Wt1 expression in metformin -treated *mdx/mTR*$^{-/-}$ mice. Metformin was orally administered into 6-month old *mdx/mTR*$^{-/-}$ mice at the dose of 500 mg/kg/day for two months. **A** Western blots to examine the expression of phosphorylated and total protein expression of p65 and IκBα in dystrophic hearts of metformin-treated *mdx/mTR*$^{-/-}$ mice. Total protein (100 μg) was loaded and α-actinin was used as a loading control. Pretreated means 6-month old *mdx/mTR*$^{-/-}$ mice prior to treatment; Untreated represents PBS-treated age- and gender-matched *mdx/mTR*$^{-/-}$ mice; Metformin means metformin-treated *mdx/mTR*$^{-/-}$ mice (the rest is the same unless otherwise specified). **B** Quantitative analysis of phosphorylated p65 ($F = 7.504$, $P = 0.023$) and IκBα ($F = 11.28$, $P = 0.009$) in dystrophic hearts ($n = 3$, $^{*}p < 0.05$; one-way ANOVA post hoc Student-Newman-Keuls test). Fold change refers to phosphorylated p65 and IκBα relative to total protein expression in metformin-treated *mdx/mTR*$^{-/-}$ mice compared to age-matched untreated controls. **C** Western blots to examine the expression of and quantitative analysis of Wt1 protein in dystrophic hearts from metformin-treated *mdx/mTR*$^{-/-}$ mice ($n = 3$, $^{*}p < 0.05$; one-way ANOVA post hoc Student-Newman-Keuls test, $F = 14.838$, $P = 0.005$). Total protein (50 μg) was loaded and GAPDH was used as a loading control. **D** Immunostaining of Wt1 in the epicardium from metformin-treated *mdx/mTR*$^{-/-}$ mice (scale bar = 100 μm). Arrowheads point to Wt1-positive epicardial cells. **E** Quantitative analysis of Wt1-positive epicardial cells in metformin-treated *mdx/mTR*$^{-/-}$ mice ($n = 5$, $^{*}p < 0.05$, $^{**}p < 0.001$; one-way ANOVA post hoc Student-Newman-Keuls test, $F = 15.029$, $P < 0.001$). Data are presented as mean ± s.e.m in (**B**), (**C**) and (**E**).

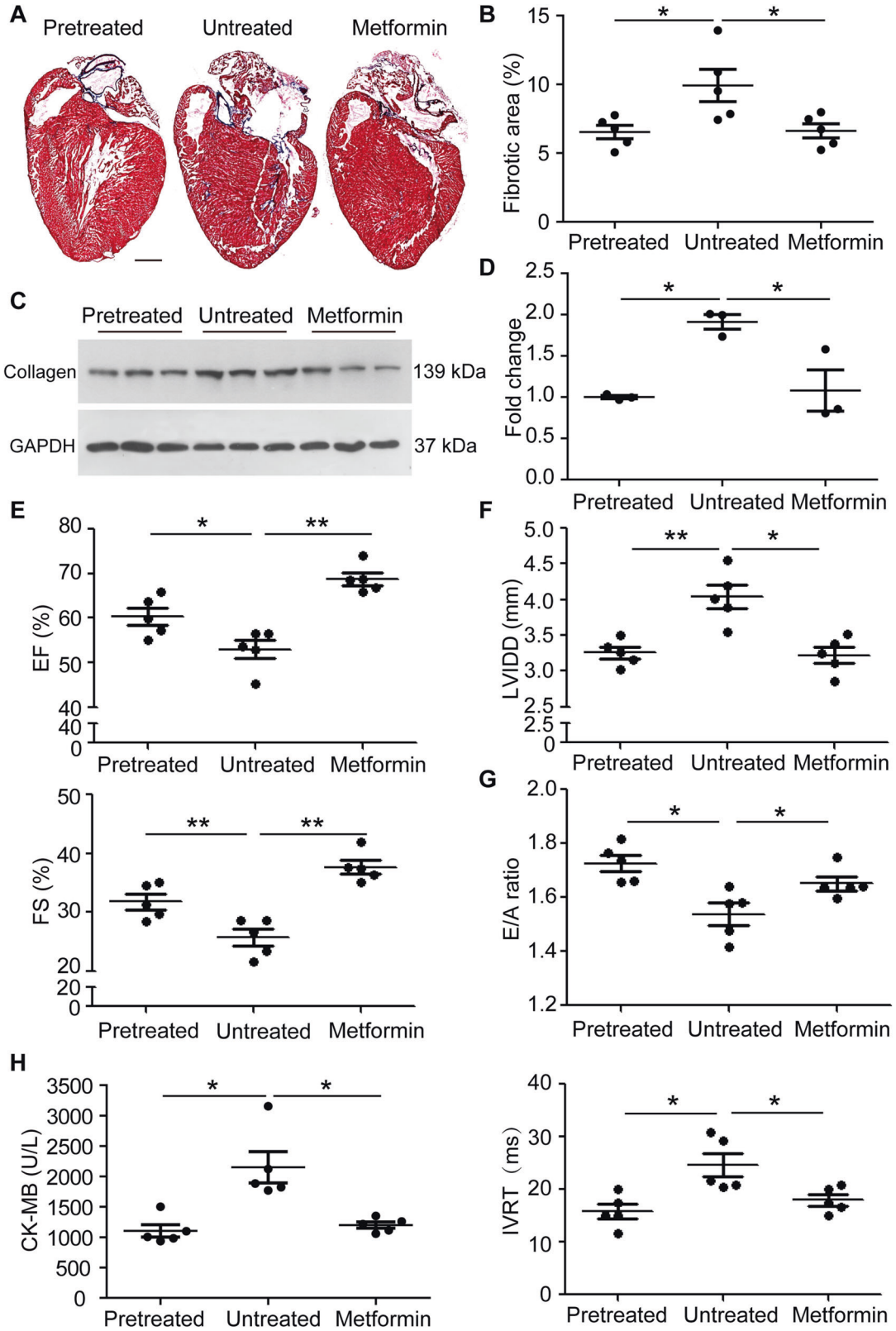

suggesting that the Wt1 mechanism is not an artifact of telomerase inhibition and is not unique only to this murine model. Intriguingly, there was a significant rise in the number of Wt1-positive epicardial cells in the epicardium of *mdx/mTR*$^{-/-}$ mice, whereas Wt1-positive epicardial cells dropped dramatically in vitro once isolated from the epicardium. We speculated that this disparity arises because chronic inflammation constantly triggers *Wt1* reactivation and subsequent proliferation of Wt1-positive epicardial cells in *mdx/mTR*$^{-/-}$ mice in vivo, while EMT transformation and differentiation of activated Wt1-positive epicardial

Fig. 6 Measurements of cardiac fibrosis and function in metformin-treated *mdx/mTR*$^{-/-}$ mice. Metformin was orally administered into 6-month old *mdx/mTR*$^{-/-}$ mice at the dose of 500 mg/kg/day for two months. **A** Representative images for collagen deposition in the whole heart from metformin-treated *mdx/mTR*$^{-/-}$ mice (scale bar = 500 μm). **B** Quantitative analysis of fibrotic (collagen-positive) areas in dystrophic hearts of metformin-treated *mdx/mTR*$^{-/-}$ mice ($n = 5$, $^{*}p < 0.05$; one-way ANOVA post hoc Student-Newman-Keuls test, $F = 5.93$, $P = 0.016$). **C** Western blots to examine the expression of collagen protein in dystrophic hearts from metformin-treated *mdx/mTR*$^{-/-}$ mice. Total protein (50 μg) was loaded and GAPDH was used as a loading control. **D** Quantitative analysis of collagen protein in dystrophic hearts ($n = 3$, $^{*}p < 0.05$; one-way ANOVA post hoc Student-Newman-Keuls test, $F = 10.785$, $P = 0.01$). Fold change refers to collagen protein expression in metformin-treated *mdx/mTR*$^{-/-}$ mice compared to age-matched untreated controls. Measurement of EF ($F = 18.26$, $P < 0.001$) and FS ($F = 31.316$, $P < 0.001$) (**E**) and LVIDD ($F = 13.664$, $P < 0.001$) (**F**), and ratio of peak early (**E**) and peak atrial filling velocity (**A**) (E/A, $F = 8.693$, $P = 0.005$) and isovolumetric relaxation time (IVRT, $F = 7.549$, $P = 0.008$) (**G**) in metformin-treated *mdx/mTR*$^{-/-}$ mouse hearts with echocardiography ($n = 5$, $^{*}p < 0.05$, $^{**}p < 0.001$; one-way ANOVA post hoc Student-Newman-Keuls test). **H** Measurement on levels of serum CK-MB in metformin-treated *mdx/mTR*$^{-/-}$ mice ($n = 5$, $^{*}p < 0.05$; one-way ANOVA post hoc Student-Newman-Keuls test, $F = 12.566$, $P = 0.001$). Data are presented as mean± s.e.m in (**B**), (**D**), (**E**), (**F**),(**G**) and (**H**).

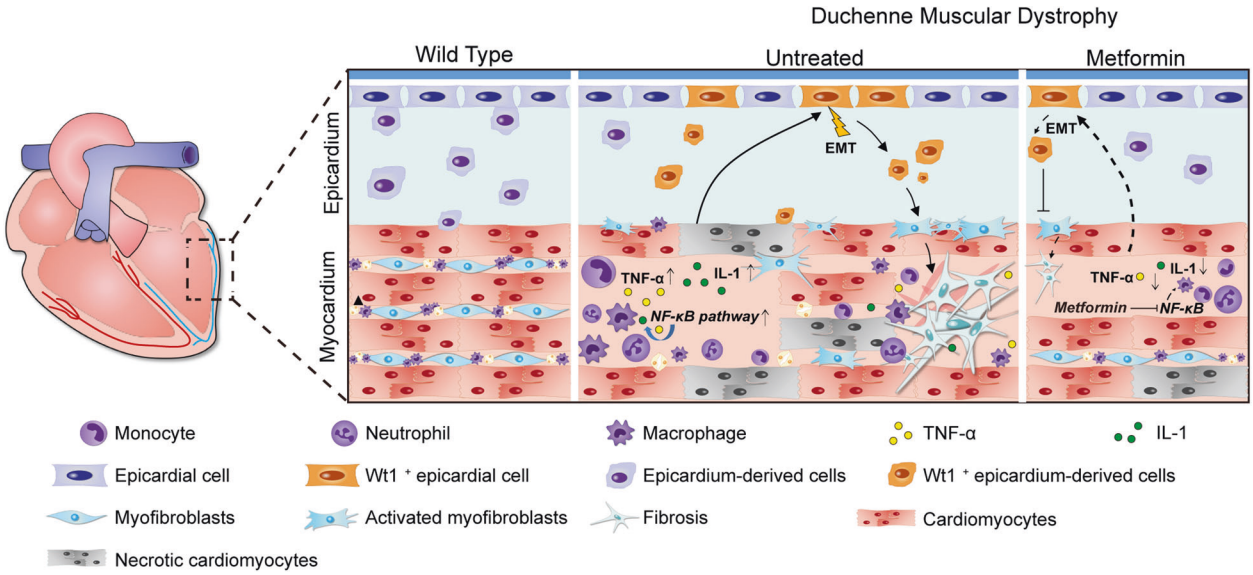

Fig. 7 Schematic to depict the mechanism of action underpinning Wt1-mediated cardiac fibrosis in dystrophic hearts. Untreated refers to untreated controls; Metformin refers to Metformin-treated; Arrows mean up- or down-regulation. EMT means epithelial-mesenchymal transition.

cells to fibroblasts in vitro in the absence of inducers [24] results in a rapid decrease in Wt1-positive epicardial cells. As cardiac fibrosis results in irreversible damage to the cardiac structure and serves to reduce cardiac function in DMD patients, identification of a pathway that can be targeted to reduce cardiac fibrosis should result in clinical improvement in DMD patients. Here, we demonstrated that *Wt1* is a potential therapeutic target. The fact that inflammatory cytokines could trigger EMT in epicardial cells in vitro suggests that differentiation to fibroblasts is decoupled from cardiac damage due to the lack of dystrophin and can cause cardiac deterioration in an inflammatory environment. To better resemble the endogenous upregulation of *Wt1*, epicardium- or epicardial cell-specific promoter for Wt1 over-expression would be preferable, however the *Wt1* promoter was proved to be promiscuous and was not tissue-restricted, despite the tissue-specific expression of Wt1 [47]. Therefore, we chose the potent CMV promoter for Wt1 over-expression, which induced significant upregulation of Wt1 in the epicardium of adult *mdx/mTR*$^{-/-}$ mice (4-month old), an age showing no elevated expression of Wt1 as demonstrated in our current study. Importantly, over-expression of Wt1 in the epicardium led to severe cardiac fibrosis in 6-month old *mdx/mTR*$^{-/-}$ mice, an extent similar to 8-month old *mdx/mTR*$^{-/-}$ mice, suggesting that Wt1 over-expression exacerbates the progression of fibrosis. Although the expression of Wt1 in the myocardium also likely contributed to cardiac fibrosis, the critical role of *Wt1* in epicardium is beyond doubt as epicardial fibrosis became severe in Wt1 over-expressing *mdx/mTR*$^{-/-}$ mice.

Metformin as an anti-hyperglycemic drug was shown to protect skeletal muscle degeneration in cardiotoxin-induced mice [48], and also long-term administration of metformin significantly ameliorated muscle pathologies in dystrophin-deficient *mdx* mice [40]. However, there was no report on the effect of metformin on dystrophic hearts, probably due to young ages of *mdx* mice used in previous studies, which show no sign of cardiac impairments [40]. Here we used metformin as an inhibitor of NF-κB [32], which has been tested in a number of human cells [32, 34, 49–51], and demonstrated the potency of metformin in improving cardiac function of dystrophic mice for the first time. As metformin appears to have multiple modes of action [52], we cannot exclude other potential mechanisms of action, but it is clear that metformin can inhibit cardiac inflammation and thus reduce cardiac fibrosis through Wt1 expression. Worth mentioning, other NF-kB inhibitors were clinically assessed in younger DMD patients (4-7-year old) with limited therapeutic effects on muscular function due to the small sample size and phenotypic variability [53–55], though there was no report on cardiac function. In addition, drugs commonly employed in cardiovascular diseases were demonstrated to function through anti-inflammation [56], thus it is possible that other anti-inflammatory agents might have similar protective effects on cardiac fibrosis of DMD. Nevertheless,

chronic administration of metformin for two months significantly prevented the development of cardiac fibrosis and inflammation in 6-month old *mdx/mTR*$^{-/-}$ mice, demonstrating the potential of metformin as a treatment option for DMD patients. Furthermore, metformin has been clinically approved and tested in DMD patients in combination with l-citrulline or arginine, with both clinical trials reporting improved muscle function in DMD patients [57, 58]. In particular, metformin with l-citrulline showed slow muscle function decline in a specific subgroup of patients with DMD, implying that individual variation might contribute to the less significant improvement on motor function in general. Although these studies failed to explore specific cardioprotective effects of metformin in DMD patients, these pre-clinical and clinical studies demonstrate the potential of metformin as a new treatment option for DMD patients. Since metformin effectively suppressed cardiac fibrosis and inflammation and resulted in improved cardiac function, co-administration of metformin with other DMD treatments, such as antisense oligonucleotides, should be an option open to clinicians.

CONCLUSION

In summary, we provide evidence that *Wt1* was upregulated in the epicardium and Wt1-positive epicardial cells contribute to cardiac fibrosis of dystrophic mice. Inflammation-induced NF-κB activation is largely responsible for the upregulation of *Wt1* in the epicardium. Importantly, metformin effectively prevented pathological progression and improved cardiac function in dystrophic mice and thus presents a potential therapeutic option for DMD.

DATA AND MATERIALS AVAILABILITY

The data underlying this article are available in the article and in its online supplementary material.

REFERENCES

1. Verhaart IEC, Aartsma-Rus A. Therapeutic developments for Duchenne muscular dystrophy. Nat Rev Neurol. 2019;15:373–86.
2. Kamdar F, Garry DJ. Dystrophin-deficient cardiomyopathy. J Am Coll Cardiol. 2016;67:2533–46.
3. Silva MC, Magalhaes TA, Meira ZM, Rassi CH, Andrade AC, Gutierrez PS, et al. Myocardial fibrosis progression in duchenne and becker muscular dystrophy: A randomized clinical trial. JAMA Cardiol. 2017;2:190–9.
4. Hinderer S, Schenke-Layland K. Cardiac fibrosis - A short review of causes and therapeutic strategies. Adv Drug Deliv Rev. 2019;146:77–82.
5. Zhou L, Lu H. Targeting fibrosis in Duchenne muscular dystrophy. J Neuropathol Exp Neurol. 2010;69:771–6.
6. Mavrogeni S, Markousis-Mavrogenis G, Papavasiliou A, Kolovou G. Cardiac involvement in Duchenne and Becker muscular dystrophy. World J Cardiol. 2015;7:410–4.
7. Smits AM, Dronkers E, Goumans MJ. The epicardium as a source of multipotent adult cardiac progenitor cells: Their origin, role and fate. Pharm Res. 2018;127:129–40.
8. Simoes FC, Riley PR. The ontogeny, activation and function of the epicardium during heart development and regeneration. Development. 2018, 145.
9. Gittenberger-de Groot AC, Winter EM, Poelmann RE. Epicardium-derived cells (EPDCs) in development, cardiac disease and repair of ischemia. J Cell Mol Med. 2010;14:1056–60.
10. Braitsch CM, Yutzey KE. Transcriptional control of cell lineage development in epicardium-derived cells. J Dev Biol. 2013;1:92–111.
11. Fang M, Xiang FL, Braitsch CM, Yutzey KE. Epicardium-derived fibroblasts in heart development and disease. J Mol Cell Cardiol. 2016;91:23–27.
12. Zhou B, Pu WT. Genetic Cre-loxP assessment of epicardial cell fate using Wt1-driven Cre alleles. Circ Res. 2012;111:e276–280.
13. Schlueter J, Brand T. Epicardial progenitor cells in cardiac development and regeneration. J Cardiovasc Transl Res. 2012;5:641–53.
14. Zhou B, Honor LB, He H, Ma Q, Oh JH, Butterfield C, et al. Adult mouse epicardium modulates myocardial injury by secreting paracrine factors. J Clin Invest. 2011;121:1894–904.
15. Sacco A, Mourkioti F, Tran R, Choi J, Llewellyn M, Kraft P, et al. Short telomeres and stem cell exhaustion model Duchenne muscular dystrophy in mdx/mTR mice. Cell. 2010;143:1059–71.
16. Dehbi M, Hiscott J, Pelletier J. Activation of the wt1 Wilms' tumor suppressor gene by NF-kappaB. Oncogene. 1998;16:2033–9.
17. Guo Z, Jing R, Rao Q, Zhang L, Gao Y, Liu F, et al. Immortalized common marmoset (Callithrix jacchus) hepatic progenitor cells possess bipotentiality in vitro and in vivo. Cell Disco. 2018;4:23.
18. Gao X, Ran N, Dong X, Zuo B, Yang R, Zhou Q, et al. Anchor peptide captures, targets, and loads exosomes of diverse origins for diagnostics and therapy. Sci Transl Med. 2018, 10.
19. Mackay AD, Marchant ED, Munk DJ, Watt RK, Hansen JM, Thomson DM, et al. Multitissue analysis of exercise and metformin on doxorubicin-induced iron dysregulation. Am J Physiol Endocrinol Metab. 2019;316:E922–E930.
20. Sicinski P, Geng Y, Ryder-Cook AS, Barnard EA, Darlison MG, Barnard PJ. The molecular basis of muscular dystrophy in the mdx mouse: A point mutation. Science. 1989;244:1578–80.
21. Tarbit E, Singh I, Peart JN, Rose'Meyer RB. Biomarkers for the identification of cardiac fibroblast and myofibroblast cells. Heart Fail Rev. 2019;24:1–15.
22. Privratsky JR, Newman PJ. PECAM-1: Regulator of endothelial junctional integrity. Cell Tissue Res. 2014;355:607–19.
23. Hinz B, Celetta G, Tomasek JJ, Gabbiani G, Chaponnier C. Alpha-smooth muscle actin expression upregulates fibroblast contractile activity. Mol Biol Cell. 2001;12:2730–41.
24. Bax NA, van Oorschot AA, Maas S, Braun J, van Tuyn J, de Vries AA, et al. In vitro epithelial-to-mesenchymal transformation in human adult epicardial cells is regulated by TGFbeta-signaling and WT1. Basic Res Cardiol. 2011;106:829–47.
25. van Tuyn J, Atsma DE, Winter EM, van der Velde-van Dijke I, Pijnappels DA, Bax NA, et al. Epicardial cells of human adults can undergo an epithelial-to-mesenchymal transition and obtain characteristics of smooth muscle cells in vitro. Stem Cells. 2007;25:271–8.
26. Osterreicher CH, Penz-Osterreicher M, Grivennikov SI, Guma M, Koltsova EK, Datz C, et al. Fibroblast-specific protein 1 identifies an inflammatory subpopulation of macrophages in the liver. Proc Natl Acad Sci USA. 2011;108:308–13.
27. Bish LT, Morine K, Sleeper MM, Sanmiguel J, Wu D, Gao G, et al. Adeno-associated virus (AAV) serotype 9 provides global cardiac gene transfer superior to AAV1, AAV6, AAV7, and AAV8 in the mouse and rat. Hum Gene Ther. 2008;19:1359–68.
28. Miyatake S, Shimizu-Motohashi Y, Takeda S, Aoki Y. Anti-inflammatory drugs for Duchenne muscular dystrophy: Focus on skeletal muscle-releasing factors. Drug Des Devel Ther. 2016;10:2745–58.
29. Viatour P, Merville MP, Bours V, Chariot A. Phosphorylation of NF-kappaB and IkappaB proteins: Implications in cancer and inflammation. Trends Biochem Sci. 2005;30:43–52.
30. Cruz-Guzman Odel R, Rodriguez-Cruz M, Escobar Cedillo RE. Systemic inflammation in Duchenne Muscular Dystrophy: Association with muscle function and nutritional status. Biomed Res Int. 2015;2015:891972.
31. Lawrence T. The nuclear factor NF-kappaB pathway in inflammation. Cold Spring Harb Perspect Biol. 2009;1:a001651.
32. Isoda K, Young JL, Zirlik A, MacFarlane LA, Tsuboi N, Gerdes N, et al. Metformin inhibits proinflammatory responses and nuclear factor-kappaB in human vascular wall cells. Arterioscler Thromb Vasc Biol. 2006;26:611–7.
33. Chen X, Li X, Zhang W, He J, Xu B, Lei B, et al. Activation of AMPK inhibits inflammatory response during hypoxia and reoxygenation through modulating JNK-mediated NF-kappaB pathway. Metabolism. 2018;83:256–70.
34. Hattori Y, Suzuki K, Hattori S, Kasai K. Metformin inhibits cytokine-induced nuclear factor kappaB activation via AMP-activated protein kinase activation in vascular endothelial cells. Hypertension. 2006;47:1183–8.
35. Zheng Y, Li P, Huang H, Ye X, Chen W, Xu G, et al. Androgen receptor regulates eIF5A2 expression and promotes prostate cancer metastasis via EMT. Cell Death Disco. 2021;7:373.
36. Kim MJ, Bible KL, Regnier M, Adams ME, Froehner SC, Whitehead NP. Simvastatin provides long-term improvement of left ventricular function and prevents cardiac fibrosis in muscular dystrophy. Physiol Rep. 2019;7:e14018.
37. Markham LW, Michelfelder EC, Border WL, Khoury PR, Spicer RL, Wong BL, et al. Abnormalities of diastolic function precede dilated cardiomyopathy associated with Duchenne muscular dystrophy. J Am Soc Echocardiogr. 2006;19:865–71.
38. Khouzami L, Bourin MC, Christov C, Damy T, Escoubet B, Caramelle P, et al. Delayed cardiomyopathy in dystrophin deficient mdx mice relies on intrinsic glutathione resource. Am J Pathol. 2010;177:1356–64.
39. Siegel AJ, Silverman LM, Holman BL. Elevated creatine kinase MB isoenzyme levels in marathon runners. Normal myocardial scintigrams suggest noncardiac source. JAMA. 1981;246:2049–51.
40. Mantuano P, Sanarica F, Conte E, Morgese MG, Capogrosso RF, Cozzoli A, et al. Effect of a long-term treatment with metformin in dystrophic mdx mice: A

reconsideration of its potential clinical interest in Duchenne muscular dystrophy. Biochem Pharm. 2018;154:89–103.
41. Rosenberg AS, Puig M, Nagaraju K, Hoffman EP, Villalta SA, Rao VA, et al. Immune-mediated pathology in Duchenne muscular dystrophy. Sci Transl Med. 2015;7:299rv294.
42. Scholz H, Kirschner KM. A role for the Wilms' tumor protein WT1 in organ development. Physiol (Bethesda). 2005;20:54–59.
43. Kasam RK, Ghandikota S, Soundararajan D, Reddy GB, Huang SK, Jegga AG, et al. Inhibition of Aurora Kinase B attenuates fibroblast activation and pulmonary fibrosis. EMBO Mol Med. 2020;12:e12131.
44. Sontake V, Shanmukhappa SK, DiPasquale BA, Reddy GB, Medvedovic M, Hardie WD, et al. Fibrocytes regulate wilms tumor 1-positive cell accumulation in severe fibrotic lung disease. J Immunol. 2015;195:3978–91.
45. Kharraz Y, Guerra J, Pessina P, Serrano AL, Munoz-Canoves P. Understanding the process of fibrosis in Duchenne muscular dystrophy. Biomed Res Int. 2014;2014:965631.
46. Duim SN, Goumans MJ, Kruithof BPT. WT1 in cardiac development and disease. In: van den Heuvel-Eibrink MM (ed). Wilms Tumor: Brisbane (AU), 2016.
47. Fraizer GC, Wu YJ, Hewitt SM, Maity T, Ton CC, Huff V, et al. Transcriptional regulation of the human Wilms' tumor gene (WT1). Cell type-specific enhancer and promiscuous promoter. J Biol Chem. 1994;269:8892–8900.
48. Langone F, Cannata S, Fuoco C, Lettieri Barbato D, Testa S, Nardozza AP, et al. Metformin protects skeletal muscle from cardiotoxin induced degeneration. PLoS One. 2014;9:e114018.
49. Ba W, Xu Y, Yin G, Yang J, Wang R, Chi S, et al. Metformin inhibits pro-inflammatory responses via targeting nuclear factor-kappaB in HaCaT cells. Cell Biochem Funct. 2019;37:4–10.
50. Sun J, Huang N, Ma W, Zhou H, Lai K. Protective effects of metformin on lipopolysaccharideinduced airway epithelial cell injury via NFkappaB signaling inhibition. Mol Med Rep. 2019;19:1817–23.
51. Zhao Y, Sun M. Metformin rescues Parkin protein expression and mitophagy in high glucose-challenged human renal epithelial cells by inhibiting NF-kappaB via PP2A activation. Life Sci. 2020;246:117382.
52. Rena G, Hardie DG, Pearson ER. The mechanisms of action of metformin. Diabetologia. 2017;60:1577–85.
53. Markati T, De Waele L, Schara-Schmidt U, Servais L. Lessons learned from discontinued clinical developments in Duchenne muscular dystrophy. Front Pharm. 2021;12:735912.
54. McDonald CM, Henricson EK, Abresch RT, Florence JM, Eagle M, Gappmaier E, et al. The 6-minute walk test and other endpoints in Duchenne muscular dystrophy: longitudinal natural history observations over 48 weeks from a multicenter study. Muscle Nerve. 2013;48:343–56.
55. Finanger E, Vandenborne K, Finkel RS, Lee Sweeney H, Tennekoon G, Yum S, et al. Phase 1 study of Edasalonexent (CAT-1004), an Oral NF-kappaB Inhibitor, in pediatric patients with duchenne muscular dystrophy. J Neuromuscul Dis. 2019;6:43–54.
56. Golia E, Limongelli G, Natale F, Fimiani F, Maddaloni V, Pariggiano I, et al. Inflammation and cardiovascular disease: From pathogenesis to therapeutic target. Curr Atheroscler Rep. 2014;16:435.
57. Hafner P, Bonati U, Erne B, Schmid M, Rubino D, Pohlman U, et al. Improved muscle function in Duchenne muscular dystrophy through L-Arginine and metformin: An investigator-initiated, open-label, single-center, proof-of-concept-study. PLoS One. 2016;11:e0147634.
58. Hafner P, Bonati U, Klein A, Rubino D, Gocheva V, Schmidt S, et al. Effect of combination l-Citrulline and Metformin treatment on motor function in patients with Duchenne muscular dystrophy: A randomized clinical trial. JAMA Netw Open. 2019;2:e1914171.

ACKNOWLEDGEMENTS

The authors acknowledge Dr. Yiqi Seow (Biomedical Sciences Institutes, A*STAR, Singapore) for critical review of the manuscript and Dr. Wenyan Niu (Tianjin Metabolic Disease Hospital, Tianjin Medical University, Tianjin, China) for assistance with the clinical biochemistry assays.

AUTHOR CONTRIBUTIONS

HY and ZG designed the project; ZG, MG, YH, GH, RJ, CL, XZ, and MZ. carried out the experiments; GF provided help with cardiac function test; FW helped with mouse breeding; ZG, MG, and HY analyzed the data; HY, ZG, and MG wrote the paper with the input from all authors.

FUNDING

This study is supported by National Key R&D Program of China (Grant No.2017YFC1001902), National Natural Science Foundation of China (Grant No. 81672124 and 81802124), Tianjin Research Innovation Project for Postgraduate Students (2020YJSB159), and Tianjin Municipal 13th five-year plan (Tianjin Medical University Talent Project).

COMPETING INTERESTS

The authors declare no competing interests.

CONSENT TO PARTICIPATE

The authors have agreed to the publication in Cell Death & Differentiation.

ADDITIONAL INFORMATION

Supplementary information The online version contains supplementary material available at https://doi.org/10.1038/s41418-022-00979-0.

Correspondence and requests for materials should be addressed to HaiFang Yin.

Reprints and permission information is available at http://www.nature.com/reprints

Publisher's note Springer Nature remains neutral with regard to jurisdictional claims in published maps and institutional affiliations.